Journal of Materials Chemistry A

Accepted Manuscript

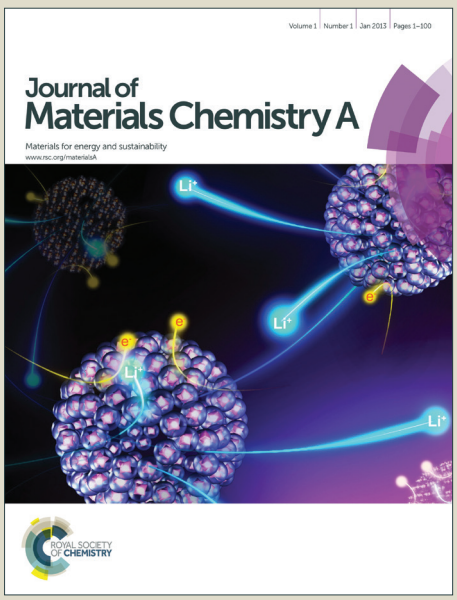

ROYAL SOCIETY OF CHEMISTRY

www.rsc.org/materialsA

Journal of Materials Chemistry A

Journal of Materials Chemistry A

Dynamic Article Links ▶

Cite this: DOI: 10.1039/c0xx00000x

www.rsc.org/xxxxxx

COMMUNICATION

High rate capability supercapacitors assembled from wet-spun graphene films with $CaCO_3$ template

Tieqi Huang,[a] Bingna Zheng,[a] Zheng Liu,[a] Liang Kou[a] and Chao Gao*[a]

Received (in XXX, XXX) Xth XXXXXXXXX 20XX, Accepted Xth XXXXXXXXX 20XX

DOI: 10.1039/b000000x

We fabricate continuous wrinkle-structured graphene film electrodes by a wet-spinning based methodology. The assembled supercapacitors exhibited excellent rate performance (79% retention from 1 to 100 A/g) with high specific capacitance (177 F/g at 1 A/g). When further functionalized with polyaniline, the electrodes maintained the wrinkled structures and exhibited the ever best rate capability (90% retention from 1 to 100 A/g) with a superior capacitance as high as 505 F/g (1 A/g).

As an emerging technology for fast energy storage, supercapacitors exhibit outstanding performance in the aspect of fast rate charging and discharging, which means they can release their energy at an amazing speed up to 10 kW/kg.[1] As a widely used material in energy conversion, graphene performs important role in the field of supercapacitors for its high specific surface area (theoretical 2630 m^2/g), exellent conductivity (> 550 S/cm) and perfect cyclic stability.[2] Graphene-based supercapacitors, which are electric double-layer capacitors (EDLCs) due to the intrinsical carbon nature, achieve much higher specific capacitance (C_s) (90~350 F/g) than other carbon based supercapacitors.[3] However, graphene sheets are easy to assemble into compact structures because of great pi-pi interaction between layers. It is hard for electrolyte to penetrate into the layers which will influence on the contact of ions with electrodes and result in poor rate capability when charging and discharging at a high current. To promote the rate performance, structure engineering was presented for improving the contact effect. Xue and coworkers made folded structured graphene paper from graphene aerogel to enlarge the interspace between graphene sheets, and the resulting supercapacitors kept 64% C_s as the current density increased from 1 A/g to 100 A/g.[4] Hu's group used MgO template to prepare graphene nanocage-based supercapacitors with controlled porous size that held 52% C_s from 1 A/g to 100 A/g.[5] Feng et al. prepared supercapacitors with vertically oriented graphene to improve the contact between graphene and current collectors, which maintained 88% C_s from 1 A/g to 100 A/g.[6] Li and coworkers introduced water or ionic liquid as spacer to separate graphene sheets with 70% ~ 80% C_s retention from 1 A/g to 100 A/g.[7,8] Despite such progresses, one big challenge is to be urgently resolved before real application of graphene-based supercapacitors: continuous and fast production of graphene film electrodes while keeping high rate capability.

Here, we develop a wet-spinning approach[9-13] to fabricate continuous graphene films containing $CaCO_3$ crystals between graphene interlayer. After removing the $CaCO_3$ template by acid-etching, wrinkled graphene film (WGF) electrodes are readily achieved. The assembled neat graphene supercapacitors show high C_s of 177 F/g at 1 A/g (141 mF/cm^2 or 403 F/cm^3), superior rate capability (79% at 100 A/g), and favorable cyclic stability (91% retention after 10000 cycles). Furthermore, we introduce a conductive polymer of polyaniline (PANI) into the wrinkled graphene films by *in situ* polymerization. The modified supercapacitors exhibit high C_s up to 505 F/g at 1 A/g and ultrahigh rate capability (90% retention from 1 A/g to 100 A/g), the best ever reported for all PANI-graphene based supercapacitors.

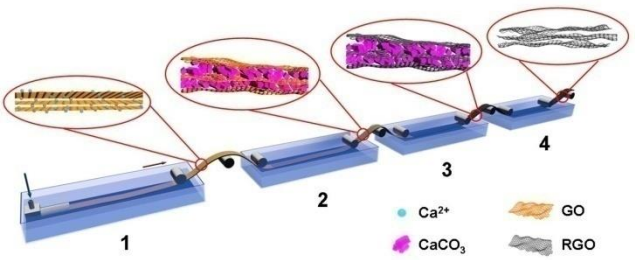

Fig.1 Continuous production of wrinkled graphene film electrodes by wet-spinning based methodology. Step **1**: wet-spinning of GO liquid crystal from a specially designed broad nozzle into a coagulation bath ($CaCl_2$ 5 wt %, ethanol: H_2O = 1:3); step **2**: *in situ* growth of calcite crystals in a 5 wt% Na_2CO_3 aqueous solution; step **3**: chemical reduction in a 20 wt% hydrazine hydrate solution at 85 °C; step **4**: etching of calcite in a 1M HCl solution. The zoom in cartoon images illustrate idealized microstructures of corresponding films.

Fig. 1 depicts the process to produce continuous graphene film electrodes on the basis of wet-spinning assembly methodology. Notably, although wet-spinning approach has been widely demonstrated as a fast and controllable way to fabricate polymer fibers, carbon nanotube fibers,[14,15] and graphene fibers,[9-13,16-20] it had never been used to prepare macroscopic porous films. Recently, our group have invented a new wet-spinning method to prepare neat graphene compact film.[21] In this work, four

continuous steps are included in the new protocol: i) wet-spinning of graphene oxide (GO) liquid crystal dope into a coagulation solution of $CaCl_2$/ethanol/H_2O to obtain Ca^{2+}-crosslinked GO hydrogel film,[9,10] ii) immersing in 5wt% Na_2CO_3 aqueous solution to form $CaCO_3$ crystals between GO sheets, iii) immersing in hot (85 °C) Hydrazine hydrate solution to reduce GO film into graphene film ($CaCO_3$-GF), iv) etching $CaCO_3$ crystals in 1M HCl solution to achieve WGF electrodes. The idealized microstructures of corresponding film are illustrated by cartoons in Fig. 1.

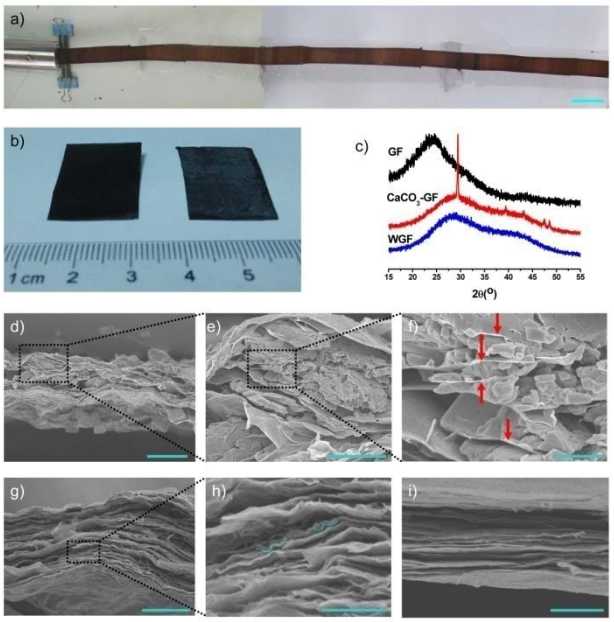

Fig.2 a) A section of continuous wet-spun GO film. b) Photograph of WGF (left) and $CaCO_3$-GF (right). c) XRD patterns of GF, $CaCO_3$-GF, and WGF. d-f) SEM images of $CaCO_3$-GF with different magnifications. g, h) SEM images of WGF. i) SEM image of GF. The arrows in f) show graphene sheets intercalated with calcite crystals. The dash lines in h) show the 'w' shape-like wrinkled graphene sheets. Scale bar: a) 2 cm, d) 20 μm, e) 2 μm, f) 1 μm, g) 2 μm, h) 500 nm, i) 2 μm.

Fig. 2a shows the continuous wet-spun GO film prepared at step i), indicating the fast productivity and fine controllability of our approach. Fig. 2b displays $CaCO_3$-GF and WGF cut from step iii) and iv), respectively. The *in situ* generation and removal of $CaCO_3$ crystal template is to create wrinkles for graphene sheets, which would be helpful for the improvement of electrochemical performance.[7,8,22] For comparison, the reduced GO films without $CaCO_3$ template (GFs) were also directly used to construct supercapacitors as control group.

Fig. 2c shows the X-ray diffraction (XRD) patterns of GF, $CaCO_3$-GF and WGF with 2θ ranging from 15° to 55°. For the normal GF film, there is a manifest peak at 24.5° which belongs to the graphene stacking structure with an interlayer spacing of 0.37 nm. By contrast, no typical peaks of graphene stacking structure are detected for both $CaCO_3$-GF and WGF, indicating amorphous microstructures for such films. The peaks corresponding to calcite $CaCO_3$ crystal (PDF card #47-1743) are found in the XRD profile of $CaCO_3$-GF, demonstrating the formation of $CaCO_3$ crystals in the interlayers of graphene films. After etching by HCl, such peaks disappear in the WGF.

The microstructures of the films were directly observed by scanning electron microscope (SEM). Fig. 2d-f shows the cross section morphology of $CaCO_3$-GF under different magnifications. The graphene sheets are well separated from each other by $CaCO_3$ particles (see the red arrows in Fig. 2f for the separated graphene sheets). The $CaCO_3$ composition was confirmed by energy dispersive spectrometer (EDS) mapping analysis (Fig. S1). Because of the intercalation of $CaCO_3$ crystals, the surface of $CaCO_3$-GF became highly rough (Fig. 2d), and its thickness was enlarged from around 3 to 20 μm. With the dissolution of $CaCO_3$ template, the WGF changed to 3.5-4.0 μm of thickness (Fig. 2g), much thinner than $CaCO_3$-GF and obvious thicker than the normal GF (Fig. 2i) due to its fluctuation microstructures. Under high magnification, we can clearly see waved or 'w' shape-like graphene sheets resulted from the etching of $CaCO_3$ template (Fig. 2h). In a closer view (Fig. S2), we can even see the concave-convex micro-structures of domain graphene and tens of nanometers cavities between graphene layers, which would be favorable to the electrochemcial property. In comparison, the graphene sheets in the normal GF are in good order and keep flat (Fig. 2i and Fig. S3).

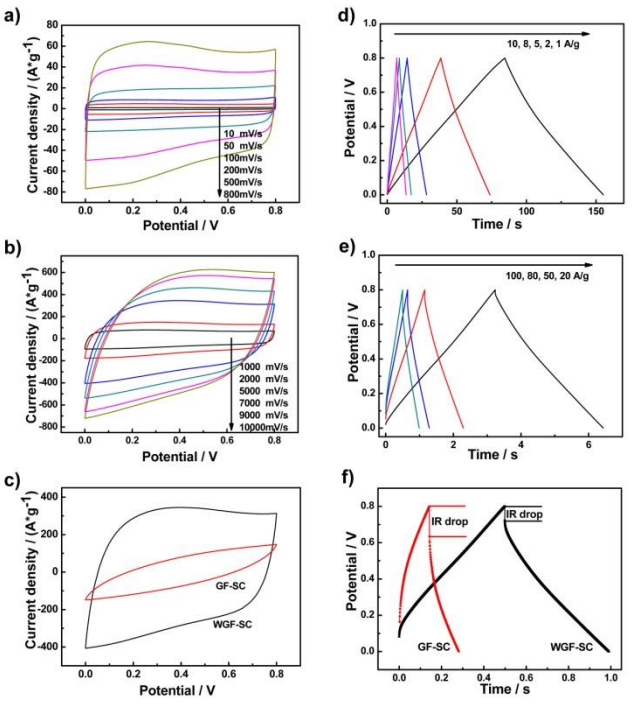

Fig.3 a) CV curves of WGF-SC from 10 to 800 mV/s; b) CV curves of WGF-SC from 1000 mV/s to 10000 mV/s; c) Comparison of CV curves of WGF-SC and GF-SC at 5000 mV/s; d) GC curves of WGF-SC at different current densities from 1 to 10 A/g; e) GC curves of WGF-SC at different high current densities from 20 to 100 A/g; f) Comparison of GC curves at the current density of 100 A/g.

The WGFs were subsequently assembled into two-electrode type supercapacitors (WGF-SCs).[23] Fig. 3a,b shows the typical cyclic voltammogram (CV) curves of WGF-SC from 10 to 10,000 mV/s. Under low scan rates (Fig. 3a), each curve of the WGF-SC is axisymmetric and shows perfect rectangle shape

which indicates good EDLC property. As scan rate increases, WGF-SC enhances to a larger area of CV curve but maintains the rectangular shape very well. When the scan rate reaches to as high as 10000 mV/s (Fig. 3b), the curve still keeps a quasirectangular shape, which is hard to realize for many carbon based electrodes.[3,24,25] By comparison, under low scan rate, e. g. 10 mV/s (Fig. S4), the two supercapacitors of both GF-SC and WGF-SC show nearly rectangle shapes of CV curves, while the shape of GF-SC is distorted into leaf-like shape under the high scan rate of 5000 mV/s (note: WGF-SC still remains good quasirectangle shape, as shown in Fig. 3c. The C_s and rate capability based on the calculation of CV curves also demonstrate the superiority of WGF-SC: the retention of WGF-SC is 47% (179 F/g at 10 mV/s, 85 F/g at 10000 mV/s), whereas GF-SC only maintains 14% (95 F/g at 10 mV/s, 13 F/g at 10000 mV/s).

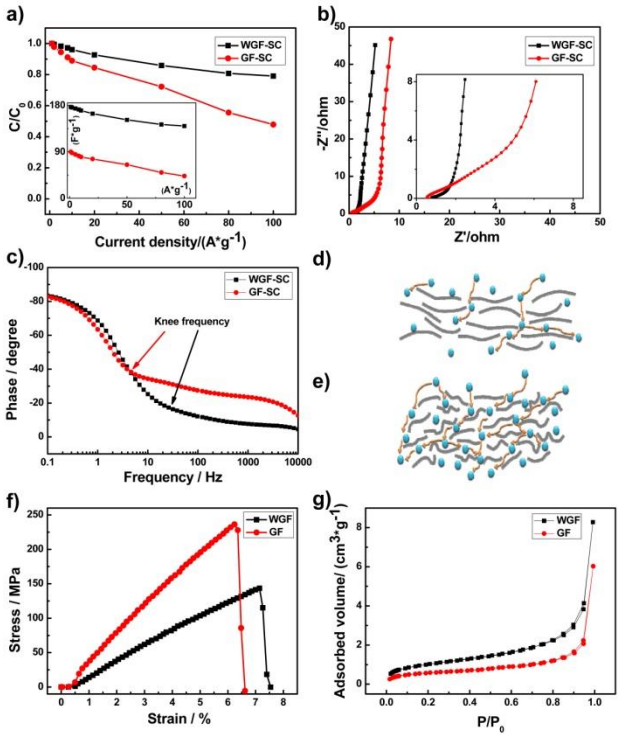

Fig.4 a) Comparison of rate capabilities of WGF-SC and GF-SC at different current densities, the insert Fig. shows specific C_s of WGF-SC and GF-SC at different current densities, C_0: C_s at the current density of 1 A/g; b) Nyquist plots of WGF-SC and GF-SC, the insert Fig. is magnified portion near the origin; c) Comparison of Bode plots of WGF-SC and GF-SC; d, e) Schematic illustration of ion transport of WGF-SC and GF-SC, respectively; f) Mechanical properties of WGF and GF; g) Nitrogen adsorption isotherms of WGF and GF.

Galvanostatic charge and discharge (GC) is another important test for supercapacitors. Fig. 3d shows that under low current density (1-10 A/g), the WGF-SC performs well symmetric linear curves during charging and discharging. As the current density increases, the shape of our WGF-SC still keeps perfect symmetric lines(Fig. 3e), which conforms good capacitive behaviour and electrochemical reversibility.[26] Compared with the GF-SC, the WGF-SC shows much better properties of EDLC. Fig. S5 shows the comparison of such two kinds of electrodes under the current density of 1 A/g. The discharge time of WGF-SC (70.8 s) is clearly larger than that of GF-SC (35.8 s), which means the storage performance of WGF-SC is better than GF-SC. As the current density increases to 100 A/g, the shape of GF-SC is distorted into asymmetric arc lines while WGF-SC remains good symmetric lines (Fig. 3f). For WGF-SC and GF-SC, their IR drops are so small that can be ignored under low current density of 1 A/g. However, when the current density increases, the IR drop enlarges with different degree for WGF-SC and GF-SC. According to Fig. 3f, WGF-SC remains small internal resistance (IR) drop even at high current density (0.08 V for 100 A/g), whereas the IR drop of GF-SC is much larger (0.17 V for 100 A/g). All these data demonstrate that the WGF-SC performs excellently in GC mearsuments. Its stability test was carried out at the current density of 10 A/g (Fig. S6). Only 9% reduction after 10000 cycles demonstrates the good cyclic stability of WGF-SC.

We assessed the rate capabilities of WGF-SC and GF-SC, which were calculated from GC measurements. At a low current density of 1 A/g, the WGF-SC shows C_s of 177 F/g (141 mF/cm^2 or 403 F/cm^3) (Fig. 4a), which is in the normal interval of 90 ~ 250 F/g for graphene based EDLCs. Notably, under a high current density of 100 A/g, the WGF-SC still shows C_s as high as 140 F/g. For the control GF-SC, C_ss at all tested current densities (90 F/g at 1 A/g and only 43 F/g at 100 A/g) are far lower than those of WGF-SC. After normalization, the comparison for the rate capability of the two electrodes is more clear (the insert in Fig. 4a). The reduction for GF-SC is 52% as the current density approaches to 100 A/g. By contrast, the WGF-SC shows only 21% reduction (79% retention) from 1 to 100 A/g, which is comparable to the best rate capabilities ever reported (52% for carbon nanocage,[5] 64% for graphene foam[4], 69% for liquid-spacer graphene film,[8] 75% for graphene gel,[15] 81% for water-spacer graphene film,[7] 88% for vertical graphene bridging[6]). Table S1 summerizes the comparison data of our WGF-SC and SCs reported previously at different high current densities, confirming the superior rate capability of WGF-SC.

Electrochemical impedance spectroscopy (EIS) was conducted on the two kinds of electrodes to investigate their resistances in the electrolyte system from 0.1 to 100 kHz. The low frequency portions of Nyquist plots of WGF-SC and GF-SC are nearly vertical to the axis of real component at low frequency (Fig. 4b), which means ideal EDLC behavior.[28] As the part of curve (slope of 1) named as Warburg-type line illustrates the ion diffusion and transport process,[29] the WGF-SC shows superior ion diffusion ability within the wrinkled graphene sheets because of the enhanced compatibility between the electrode and electrolyte. The insert in Fig. 4b is the magnified portion of the Nyquist plots near the origin to deeply understand the behavior of capacitive impedance. Our WGF-SC still shows no obvious Warburg-type line at such high frequency whereas GF-SC shows clearly. Meanwhile, the loop size at high frequency also demonstrates the charge-transport resistance and interfacial resistance. The negligible loop of WGF-SC indicates good connection of the WGF with electrolyte and fast transmission of ions and electrons because of the unique wrinkled graphene sheet microstructures.[6] The intercepts of prolonged WGF-SC and GF-SC at low frequency region with the real axis, which can be defined as equivalent series resistances (ESR), are 1.7 ohm and 5.2 ohm,

respectively. As the two supercapacitors are assembled with the same electrolyte solution of 1 M H_2SO_4. It demonstrates that the ion transmission in WGF is much more effective than the ion transmission in GF. The critical frequency (knee frequency) in the Nyquist plot means where all surface area is accessed.[30] As shown in Fig.4c, the higher knee frequency of WGF-SC (31.6 Hz) indicates that wrinkled graphene sheets strongly favor power capability, compared with GF-SC (4.6 Hz).

We suggested two different ion transmission paths for WGF-SC and GF-SC, respectively. As shown in Fig. 4d, the template-induced disorder folded graphene sheets contact well with electrolyte and shorten the path for ion transmission. For GF-SC, GF remains more restaking portions than WGF and it requests longer time for ion charging and discharging because ions need to come across the long distance of flat graphene sheets (Fig. 4e).

To verify the wrinkled structure in the WGF, we also tested its mechanical performance. Fig. 4f shows the different mechanical properties of WGF and GF, respectively. WGF shows lower stress (144 MPa) for its loose wrinkled structure while the compact-structured GF shows higher stress (236 MPa) with strong pi-pi interaction between interlayers. Moreover, the strain of WGF (7.14%) is higher than GF (6.24%) due to the unfolding process of wrinkled graphene sheets during streching.

The nitrogen cryoadsorption isotherms are shown in Fig. 4g, and both WGF and GF exhibit Type III isotherm. The Brunauer–Emmett–Teller (BET) surface area of WGF (158 m^2/g) is obviously larger than that of GF (71 m^2/g), which means the contact area for ion intercalation and deintercalation of WGF is larger than GF. The pore distrbutions are shown in Fig. S7 (for WGF) and Fig. S8 (for GF). The total pore volume of WGF (0.54 cm^3/g) is also lager than that of GF (0.31 cm^3/g), demonstrating the loose space for ion transmission in WGF. This is consistent with the above results.

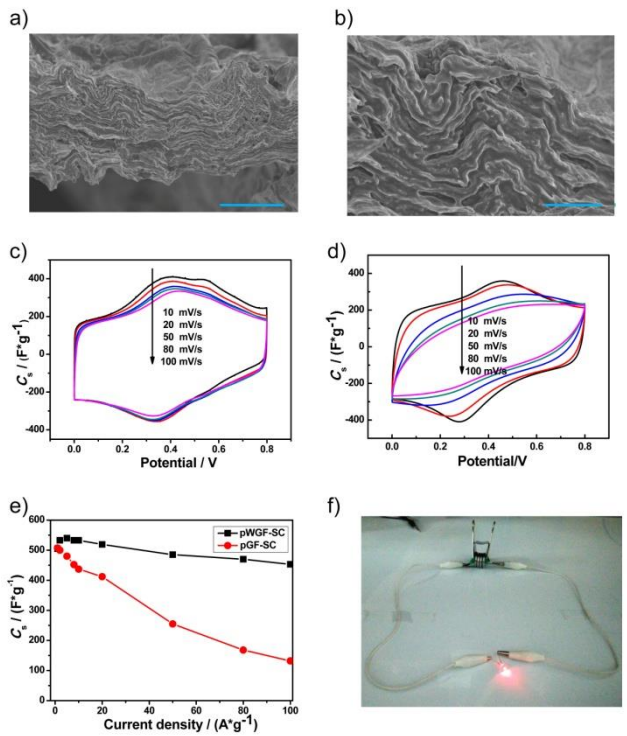

Fig.5 a, b) SEM images of pWGF at different magnifications, scale bar: 10 μm (a), 2 μm (b); c) CV curves of pWGF-SC with different scan rates ranges from 10 to 100 mV/s; d) CV curves of pGF-SC with different scan rates ranges from 10 to 100 mV/s; e) Comparison of C_ss of pWGF-SC and pGF-SC; f) lighting of a red LED by series-connected 4 cells of pWGF-SC.

The C_s of EDLCs is relatively limited for their intrinsic physical mechanism.[25,31] Many efforts have been made to improve the capacitance of EDLCs, among which introducing pseudocapacitance is the most effective method (including doping of conductive polymers[32-37] and metal oxides[38-44]). However, pseudocapacitance always degrades the rate performance of electrodes and results in low capacitance under high current.[3] So to achieve high rate capability while keeping large capacitance is a challenge for electrochemical supercapacitors. Wei and coworkers introduced PANI nanowire arrays into 3D porous graphene networks and the resulting supercapacitors showed good rate performance (89% maintained from 0.5 to 10 A/g).[22] In this paper, as a good EDLC with superior rate capability, WGF was also used as substrate to grow PANI for further increasing the performance of supercapacitors.

Fig. 5a shows the SEM image of PANI-functionalized WGF (pWGF) prepared by *in situ* polymerization of aniline in the WGF networks. The height of films increased from original 4 μm to 10 μm due to the intercalation of PANI. The sheets of pWGF look much more plump than the case of neat WGF and many nanoparticles are clearly seen on the graphene sheets (Fig. S9), which demonstrates the successful dopping of PANI. Under higher magnification (Fig. 5b), numerous wrinkles in pWGF are observed which inherit from the original WGF. Fig. 5c shows the CV curves of pWGF-SC from 10 to 100 mV/s. The two pairs of peaks illustrate the redox reactions of PANI corresponding to the leucoemeraldine-emeraldine transition and the emeraldine-pernigraniline transition.[42] Significantly, the shape of the curves changes little upon scan rates, which means our pWGF-SC still response quickly even at high scan rates.[6] As a comparison, the curves of PANI-functionalized GF-SC (pGF-SC) distort seriously as the scan rate increases and no obvious redox peaks can be found in the curve of 100 mV/s, indicating its inferior behavior of rate capability.

Fig. 5d shows the rate capabilities of pWGF-SC and pGF-SC caculated by GC measurements. At 1 A/g, the C_s of pWGF-SC (505 F/g) nearly equals to that of pGF-SC (507 F/g), showing that the two electrodes both perform well under low current density (Fig. S10). The largely increased C_s (from 177 F/g to 505 F/g) is mainly resulted from the great effect of pseudocapacitance of PANI. Both the curves of pWGF-SC and pGF-SC show two typical portions: the 0.8 V~0.45 V portion attributes to EDLC and 0.45 V~0 V portion attributes mainly to pseudocapacitance of PANI.[35] As the current density increases, the C_s of pGF-SC decreases much faster than that of pWGF-SC. At 100 A/g, the pWGF-SC shows C_s as high as 453 F/g and remains 90% of C_s at 1 A/g, whereas pGF-SC loses 74% (retains only 26%) of C_s at 1 A/g and decreases to 132 F/g. The IR drop of pGF-SC (0.13 V) is more than twice of that of pWGF-SC (0.06 V), and the GC curve of pGF-SC is distorted at 100 A/g (Fig. S11). All these data demonstrate the excellent rate capability of the pWGF-SC. The wrinkles of pWGF contribute to the fast transmission paths for electrolytes and good connection for ions and graphene sheets, as

the same with the case of original WGF. Notably, the conductivity of pWGF is better than WGF because the loose structure turns into more compact structure with the PANI as filler and connector. As shown in Fig. S12, the ESR of pWGF-SC is only 1.1 ohm, which is much lower than that of WGF-SC (1.7 ohm). The rate capability also benefits from the increased conductivity. As for pGF, the microstructure (Fig. S13) shows that the PANI's growth mainly occurs outside the film because of the compact graphene sheets of GF are hard to penetrate.

Table S2 lists the C_ss and rate capacities of our work and previous supercapacitors composed of PANI and RGO. The C_s value (505 F/g) of our pWGF-SC is at the top class, and its rate capability (100% at 20 A/g, 96% at 50 A/g, 90% at 100 A/g) is the best for all PANI-RGO based supercapacitors. In addition, the cycling charge and discharge test (Fig. S14) demonstrates the good cyclic stability (90% retention after 5000 cycles at 10 A/g) of our pWGF-SC.

We also tried to make use of this good energy storage material and manufactured devices for lighting up LEDs. We cut pWGF into circles with radius of 0.5 cm and assembled them into two-electrode cell in 1 M H_2SO_4. Four cells were connected in series, supplying a large voltage which was required by red LED (operating voltage > 2.0 V). After charging for 30 s using a 3.8 V power source, the device lighted up a red LED for more than 2 minutes (Fig. 5f). After lighting a green LED (operating voltage > 3.0 V) till it extinguished (~30 s), we charged the device again for 30 s and it lighted this green LED for 30 s once more. We tried such charging and lighting process for hundreds of times. This demonstrates that our devices can be recyclably used in real applications.[45]

Conclusions

In conclusion, we created a wet-spinning based methodology to continuously produce wrinkled graphene film electrodes by wet-spinning of GO liquid crystal followed by *in situ* growth and etching of calcite crystals between graphene interlayers. Because of the unique wrinkled microstructures of graphene sheets that enable faster ion transmission, the assembled WGF-SCs showed excellent rate capability (79% from 1 to 100 A/g) with good specific capacitance (177 F/g) and fine cycling stability (91% after 10,000 times). When further functionalized the wet-spun graphene film electrodes with PANI by *in situ* polymerization of aniline, the pWGFs inherited the wrinkled structures from the original WGFs. The resulting pWGF-SC exhibited the ever best rate capability (100% at 20 A/g, 96% at 50 A/g, and 90% at 100 A/g compared with the capacitance at 1 A/g) with a superior capacitance as high as 505 F/g (1 A/g). Our approach opens the avenue to scalable fabrication and application of high performance graphene-based supercapacitors.

Acknowledgements

This work is supported by the National Natural Science Foundation of China (no. 21325417 and no. 51173162), Fundamental Research Funds for the Central Universities (no. 2013XZZX003), and Huawei Innovation Research Program.

Notes and references

[a] *MOE Key Laboratory of Macromolecular Synthesis and Functionalization, Department of Polymer Science and Engineering, Zhejiang University, 38 Zheda Road, Hangzhou 310027, P. R. China.*
Email: chaogao@zju.edu.cn

† Electronic Supplementary Information (ESI) available: The experimental details for preparation, characterization and additional results and discussion. See DOI: 10.1039/b000000x/

1 P. Simon, Y. Gogotsi, *Nat. Mater.* 2008, **7**, 845.
2 Y. Zhu, S. Murali, W. Cai, X. Li, J. W. Suk, J. R. Potts, R. S. Ruoff, *Adv. Mater.* 2010, **22**, 3906.
3 Y. Huang, J. Liang, Y. Chen, *Small* 2012, **8**, 1805.
4 F. Liu, S. Song, D. Xue, H. Zhang, *Adv. Mater.* 2012, **24**, 1089.
5 K. Xie, X. Qin, X. Wang, Y. Wang, H. Tao, Q. Wu, L. Yang, Z. Hu, *Adv. Mater.* 2012, **24**, 347.
6 Z. Bo, W. Zhu, W. Ma, Z. Wen, X. Shuai, J. Chen, J. Yan, Z. Wang, K. Cen, X. Feng, *Adv. Mater.* 2013, **25**, 5799.
7 X. Yang, J. Zhu, L. Qiu, D. Li, *Adv. Mater.* 2011, **23**, 2833.
8 X. Yang, C. Cheng, Y. Wang, L. Qiu, D. Li, *Science* 2013, **341**, 534.
9 Z. Xu, C. Gao, *ACS Nano* 2011, **5**, 2908.
10 Z. Xu, C. Gao, *Nat. Commun.* 2011, **2**, 571.
11 Z. Xu, Y. Zhang, P. Li, C. Gao, *ACS Nano* 2012, **6**, 7103.
12 Z. Xu, H. Sun, X. Zhao, C. Gao, *Adv. Mater.* 2013, **25**, 188.
13 L. Kou, T. Huang, B. Zheng, Y. Han, X. Zhao, K. Gopalsamy, H. Sun, C. Gao, *Nat. Commun.* 2014, **5**,3754.
14 N. Behabtu, M. J. Green, M. Pasquali, *Nano Today* 2008, **3**, 24.
15 N. Behabtu, C. C. Young, D. E. Tsentalovich, O. Kleinerman, X. Wang, A. W. K. Ma, E. A. Bengio, R. F. ter Waarbeek, J. J. de Jong, R. E. Hoogerwerf, S. B. Fairchild, J. B. Ferguson, B. Maruyama, J. Kono, Y. Talmon, Y. Cohen, M. J. Otto, M. Pasquali, *Science* 2013, **339**, 182.
16 K. Gopalsamy, Z. Xu, B. Zheng, T. Huang, L. Kou, X. Zhao, C. Gao, *Nanoscale* 2014, **6**, 8595**.**
17 B. Zheng, T. Huang, L. Kou, X. Zhao, K. Gopalsamy, C. Gao, *J. Mater. Chem. A* 2014, **2**, 9736.
18 Y. Zhao, C. Jiang, C. Hu, Z. Dong, J. Xue, Y. Meng, N. Zheng, P. Chen, L. Qu, *ACS Nano* 2013, **7**, 2406.
19 Z. Xu, Z. Liu, H. Sun, C. Gao, *Adv. Mater.* 2013, **25**, 3249.
20 T. Huang, B. Zheng, L. Kou, K. Gopalsamy, Z. Xu, C. Gao, Y. Meng, Z. Wei, *RSC Adv.* 2013, **3**, 23957.
21 Liu, Z.; Li, Z.; Xu, Z.; Xia, Z.; Hu, X.; Kou, L.; Peng, L.; Wei, Y.; Gao, C. *Chem. Mater.* 2014, 10.1021/cm5033089.
22 Y. Meng, K. Wang, Y. Zhang, Z. Wei, *Adv. Mater.* 2013, **25**, 6985.
23 V. Khomenko, E. Frackowiak, F. Béguin, *Electrochim. Acta* 2005, **50**, 2499.
24 X. Cao, Z. Yin, H. Zhang, *Energ. Environ. Sci.* 2014, **7**, 1850.
25 A. G. Pandolfo, A. F. Hollenkamp, *J. Power Sources* 2006, **157**, 11.
26 R. Li, X. Ren, F. Zhang, C. Du, J. Liu, *Chem. Commun.* 2012, **48**, 5010.
27 U. N. Maiti, J. Lim, K. E. Lee, W. J. Lee, S. O. Kim, *Adv. Mater.* 2014, **26**, 615.
28 B. Hsia, J. Marschewski, S. Wang, J. B. In, C. Carraro, D. Poulikakos, C. P. Grigoropoulos, R. Maboudian, *Nanotechnology* 2014, **25**, 055401.
29 T. Y. Kim, H. W. Lee, M. Stoller, D. R. Dreyer, C. W. Bielawski, R. S. Ruoff, K. S. Suh, *ACS Nano* 2010, **5**, 436.
30 Z. Bo, Z. H. Wen, H. Kim, G. H. Lu, K. H. Yu, J. H. Chen, *Carbon* 2012, **50**, 4379.
31 E. Frackowiak, F. Béguin, *Carbon* 2001, **39**, 937.
32 L. Liu, Z. Niu, L. Zhang, W. Zhou, X. Chen, S. Xie, *Adv. Mater.* 2014, **26**, 4855.
33 S. Biswas, L. T. Drzal, *Chem. Mater.* 2010, **22**, 5667.
34 P. A. Mini, A. Balakrishnan, S. V. Nair, K. R. V. Subramanian, *Chem. Commun.* 2011, **47**, 5753.
35 Q. Wu, Y. Xu, Z. Yao, A. Liu, G. Shi, *ACS Nano* 2010, **4**, 1963.
36 J. Xu, K. Wang, S. Z. Zu, B. H. Han, Z. Wei, *ACS Nano* 2010, **4**, 5019.
37 K. Zhang, L. L. Zhang, X. S. Zhao, J. Wu, *Chem. Mater.* 2010, **22**, 1392.
38 S. Chen, J. Zhu, X. Wu, Q. Han, X. Wang, *ACS Nano* 2010, **4**, 2822.

39 Q. Cheng, J. Tang, J. Ma, H. Zhang, N. Shinya, L. C. Qin, *Carbon* 2011, **49**, 2917.

40 G. Yu, L. Hu, N. Liu, H. Wang, M. Vosgueritchian, Y. Yang, Y. Cui, Z. Bao, *Nano Lett.* 2011, **11**, 4438.

41 X. Cao, Y. Shi, W. Shi, G. Lu, X. Huang, Q. Yan, Q. Zhang, H. Zhang, *Small* 2011, **7**, 3163.

42 Y. L. Chen, Z. A. Hu, Y. Q. Chang, H. W. Wang, Z. Y. Zhang, Y. Y. Yang, H. Y. Wu, *J. Phys. Chem. C* 2011, **115**, 2563.

43 X. Dong, Y. Cao, J. Wang, M. B. Chan-Park, L. Wang, W. Huang, P. Chen, *RSC Adv.* 2012, **2**, 4364.

44 Z. S. Wu, D. W. Wang, W. Ren, J. Zhao, G. Zhou, F. Li, H. M. Cheng, *Adv. Funct. Mater.* 2010, **20**, 3595.

45 J. Yan, Q. Wang, T. Wei, Z. Fan, *Adv. Energy Mater.* 2014, **4** (DOI: 10.1002/aenm.201300816.)